## Title

Tracking Active Phase Behavior on Boron Nitride during the Oxidative Dehydrogenation of Propane Using Operando X–ray Raman Spectroscopy



## Journal

Journal of the American Chemical Society, 145(47)

## ISSN

0002-7863

## Authors

Cendejas, Melissa C
Mellone, Oscar A Paredes
Kurumbail, Unni
et al.

## Publication Date

2023-11-29

## DOI

10.1021/jacs.3c08679

# Tracking Active Phase Behavior on Boron Nitride during the Oxidative Dehydrogenation of Propane Using Operando X-Ray Raman Spectroscopy

Melissa C. Cendejas,[‡ †1] Oscar A. Paredes Mellone,[‡2] Unni Kurumbail,[3] Zisheng Zhang,[4] Jacob H. Jansen,[1] Faysal Ibrahim,[1] Son Dong,[1] John Vinson[5], Anastassia N. Alexandrova,[4] Dimosthenis Sokaras,*[2] Simon R. Bare,*[2] Ive Hermans*[1,3,6]

[1]Department of Chemistry, University of Wisconsin – Madison, Madison, Wisconsin 53706, United States; [2]Stanford Synchrotron Radiation Lightsource, SLAC National Accelerator Laboratory, Menlo Park, California 94025, United States; [3]Department of Chemical and Biological Engineering, University of Wisconsin – Madison, Madison, Wisconsin 53706, United States; [4]Department of Chemistry and Biochemistry, University of California Los Angeles, Los Angeles, California 90095, United States; [5]Material Measurement Laboratory, National Institute of Standards and Technology, Gaithersburg, Maryland 20899, United States; [6]Wisconsin Energy Institute, University of Wisconsin – Madison, Madison, Wisconsin 53706, United States.

**ABSTRACT:** Hexagonal boron nitride (hBN) is a highly selective catalyst for the oxidative dehydrogenation of propane (ODHP) to propylene. Using a variety of *ex situ* characterization techniques, the activity of the catalyst has been attributed to the formation of an amorphous boron oxyhydroxide surface layer. The ODHP reaction mechanism proceeds via a combination of surface mediated and gas phase propagated radical reactions with the relative importance of both depending on the surface-to-void-volume ratio. Here we demonstrate the unique capability of *operando* X-ray Raman spectroscopy (XRS) to investigate the oxyfunctionalization of the catalyst under reaction conditions (1 mm outer diameter reactor, 500 °C to 550 °C, $P$ = 30 kPa $C_3H_8$, 15 kPa $O_2$, 56 kPa He). We probe the effect of a water cofeed on the surface of the activated catalyst and find that water removes boron oxyhydroxide from the surface, resulting in a lower reaction rate when the surface reaction dominates and an enhanced reaction rate when the gas phase contribution dominates. Computational description of the surface transformations at an atomic-level combined with high precision XRS spectra simulations with the OCEAN code rationalize the experimental observations. This work establishes XRS as a powerful technique for the investigation of light element-containing catalysts under working conditions.

## INTRODUCTION

Hexagonal boron nitride (hBN), and other boron-containing materials (e.g., metal borides, $B_4C$, elemental boron, and boron supported on silica, carbon, and alumina) are highly selective catalysts for the oxidative dehydrogenation of propane (ODHP), exhibiting exceptionally high propylene selectivity.[1–4] Propylene is the second largest organic chemical by mass (2017 global market: 130 Mt/year),[5] currently produced in endothermic cracking or dehydrogenation processes. Exothermic technologies such as ODHP with the potential to produce propylene at a lower energy cost are therefore greatly desired.[6] The high alkene selectivity displayed by B-based catalysts compared to hitherto investigated materials has made the origin of their catalytic performance a subject of significant interest.

Catalytic activity on these boron materials is attributed to the formation of an amorphous boron oxyhydroxide phase with the general formula $B_2(OH)_{2x}O_{3-x}$ ($x \leq 3$).[7,8] For hBN, the formation of this oxyhydroxide phase is associated with an induction period during which the propane conversion steadily increases before reaching steady state.[8,9] The oxyfunctionalized boron phase is highly dynamic under ODH reaction conditions, acting as a liquid phase catalyst supported on hBN.[10] This molten phase readily restructures and can generate metastable boron sites that are not accessible at room temperature.[11,12] Extensive *ex situ* characterization has been conducted with the aim of identifying structure-performance relationships.[7–9,13–22] For example, B-OH content has been correlated with catalytic activity[20] while the details of the extended boron structure (e.g., ring or linear) continue to be the subject of ongoing research. However, the nature of the active phase is such that the species present under reaction conditions are distinct from those present on the thermally relaxed surface as observed with *ex situ* techniques, making *operando* studies imperative.

The reaction kinetics of ODH over hBN have been well established as a foundation to investigate the underlying mechanism.[2,23–27] The reaction proceeds via a radical mechanism, presumably initiated by the surface.[24–27] Reactor parameters (*e.g.,* geometry and void space) have a large effect on the reaction rate.[24] Notably, while keeping the amount of hBN constant, the reactivity scales linearly with the catalyst bed volume, with larger volumes affording higher activity. The addition of 3 % to 20 % water vapor

by volume to the reaction feed enhances the reaction rate without impacting product selectivity, indicating that water enhances the flux of existing reaction pathways.[25] Therefore, it was hypothesized that a main role of water is to increase the radical pool concentration.[25] Additionally, the reaction shows a first-order rate dependence in water and it was suggested that water can help dehydrate the surface to regenerate active species, playing a role in the rate determining step. Previous work showed that boron oxide can be hydrolyzed from the surface of silica-supported boron materials in a post-reaction washing step, resulting in deactivated catalysts with greatly decreased boron content.[13] However, the effect of water vapor on the surface of hBN during reaction has not yet been experimentally investigated and is addressed in this work.

Only a few *in situ* studies of this catalytic system have been reported, owing to harsh reaction conditions (>450 °C, $O_2$, $C_3H_8$) in combination with the difficulties of analyzing the light elements that comprise the active phase (*i.e.,* oxygen and boron).[3,4,28,29] *In situ* vibrational spectroscopy (IR and Raman) has been used with limited success, correlating B-O and B-OH features with catalytic activity.[3,4] Synchrotron vacuum ultraviolet (SVUV) radiation has also been used to confirm the presence of radical species during ODHP.[28,29] However, the conditions used in the SVUV experiment (*i.e.,* pressure) are far from those used in the actual catalytic testing, complicating the connection to the observed reaction kinetics. Moreover, the need for UV irradiation can likely trigger undesired side reactions like the dissociation of propyl radicals, leading to perturbed observations. The analytical methods applied to this catalyst system thus far have been limited due to (i) their insensitivity to light elements, (ii) their inability to obtain site-specific information, and (iii) their inability to mirror laboratory testing conditions.

X-Ray absorption spectroscopy (XAS) is a powerful tool for studying heterogenous catalysts under realistic working conditions. Such studies provide detailed element-specific atomistic information about the average local geometry, oxidation state, and coordination environment of the element being probed. Light elements, such as B, N, C, and O, have their absorption edges in the soft X-ray (<1 keV) regime. The need for soft X-rays limits the types of experiments that can be performed, as their short path length coupled with the short mean free path of the emitted electrons, necessitates measurements in (near-)vacuum environments.

X-Ray Raman spectroscopy (XRS) measures the energy loss (inelastic scattering) of a monochromatic hard X-ray (*ca.* 6.5 keV in our case), and for low momentum transfers, provides XAS-equivalent information.[30–33] Because the energy transfer from a hard X-ray is measured, XRS enables the measurement of the K-edge of light elements under actual catalytic reaction conditions instead of vacuum. Thus, XRS allows for studies of light element-containing catalysts under true working conditions while simultaneously monitoring the reaction products (*i.e., operando*). The use of XRS has been limited, owing to the small inelastic scattering cross section, and is only made possible by high flux beamlines at synchrotrons, as well as the development of high efficiency and high-energy-resolution spectrometers with a large solid angle. This technique is at the forefront of *in situ* spectroscopy and has been used to study intercalation in hydrogen sorption and battery materials.[34–38] The application of XRS in the *operando* study of heterogenous catalysts is still in its infancy but holds great promise.[39]

In this study, we track boron oxyhydroxide formation and behavior on hBN during catalyst induction, steady state operation, and during water cofeeding cycles using *operando* XRS. We probe the effect of a water cofeed on the surface of the activated catalyst and find that water removes bulk oxide from the surface, resulting in a lower reaction rate when the surface reaction dominates and an enhanced reaction rate when the gas phase contribution dominates. X-ray Raman spectra of oxyfunctionalized hBN at room temperature and elevated temperatures show subtle spectral changes to both the hBN and oxide features. We rationalize these subtle changes in X-ray Raman spectra using systematic *ab initio* calculations of XRS for metastable structure candidates determined from grand canonical simulations of boron oxyhydroxide species present under ODHP reaction conditions.

## RESULTS AND DISCUSSION

**Observing hBN Oxyfunctionalization During the Catalyst Induction Period.** hBN undergoes a sample-dependent induction period of up to several hours during which the propane conversion steadily increases before reaching a steady state (Figure 1a).[9,10] The exact shape and duration of the induction period depend on the reaction conditions. Based on *ex situ* characterization, this induction period can be attributed to the formation of the boron oxyhydroxide phase ($B_2(OH)_{2x}O_{3-x}$ ($x < 3$)) necessary for catalytic activity.[8,10] While there has been much debate about the active site structure, there is a general agreement that amorphous boron oxyhydroxide is required to achieve the catalytic activity typical for boron-based catalysts. Therefore, understanding the formation and behavior of the oxyhydroxide phase is crucial to understanding this exciting class of catalysts. We first use *operando* XRS to observe the formation of boron oxyhydroxide during the catalyst induction period of hBN.

Since XRS is a bulk-sensitive probe while catalysis is a surface phenomenon, a study of traditional bulk hBN would be entirely dominated by its bulk contribution. To increase the active surface area and achieve enhanced signal from the surface, exfoliated hBN nanosheets (hBNNS, Figure S1) were used in this study (see Supporting Information). The hBNNS sample (undiluted powder) was packed into a 1mm outer diameter (o.d.) quartz capillary tube to give a 5mm length catalyst bed. The packed quartz capillary (Figure S2) was placed in the flow cell[40] and mounted at beamline 15-2 at the Stanford Synchrotron Radiation Lightsource (SSRL) with a mass spectrometer (MS) attached to the reactor outlet.

At room temperature under a flow of synthetic air (20% $O_2$ by volume in He), the X-ray Raman spectrum of hBNNS exhibits a strong, sharp peak at 192.08 eV and a set of broader features above 197 eV (Figure 1b black spectrum).

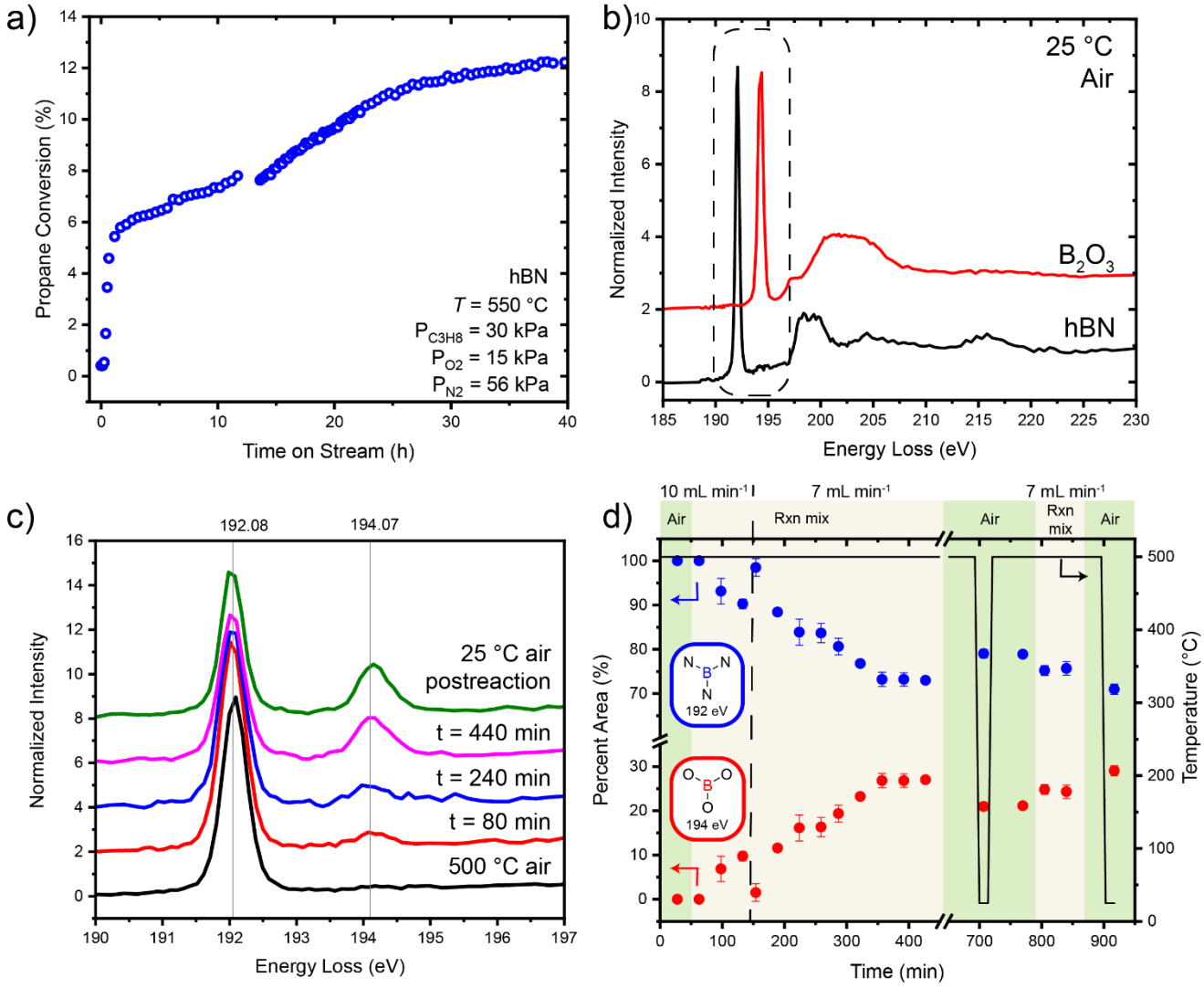


**Figure 1.** (a) Plot of propane conversion as a function of time on stream for hBN during propane ODH measured in a laboratory reactor (7 mm internal diameter); (b) Room temperature X-ray Raman spectrum of the B K-edge of hBNNS. The dashed box indicates the portion of the spectra shown in (c); (c) representative normalized *in situ* X-Ray Raman spectra of the B K-edge of hBNNS during propane ODH; (d) Percent areas of the [$BN_3$] (blue dots) and [$BO_3$] (red peaks) peaks over the course of the *operando* reaction. The green shaded areas are spectra recorded in synthetic air (20% $O_2$/He) and the beige shaded areas are recorded under reaction conditions (2:1 $C_3H_8$:$O_2$). The dashed black line indicates a change in flow rate from 10 mL $min^{-1}$ to 7 mL $min^{-1}$ and the solid black line shows the reaction temperature. The error bars in (d) are the standard deviation from averaging 3 to 5 individual scans.

The 192.08 eV feature is attributed to B 1s → π* transition in hBN ([$BN_3$] species); transitions to σ* and π* states contribute to the features above 197 eV.[41] This spectrum agrees well with results from XRS, soft XAS, and electron energy loss spectroscopy (EELS) reported in the literature.[8,41] Furthermore, the relative spectral weights of the sharp peak at 192.08 eV and the broader feature above 197 eV is a clear indication that the XRS exhibit a dominant contribution of the momentum transfer vector q parallel to the c axis.[41,42] $B_2O_3$ (Figure 1b, red spectrum) exhibits a strong sharp peak at 194.37 eV ([$BO_3$] species) and a set of broader features above 196 eV.

The sample was heated from room temperature to 500 °C (at 10 °C $min^{-1}$) under a flow of synthetic air (black trace in Figure 1c). After the temperature stabilized, propane was added into the feed in a 2:1 $C_3H_8$:$O_2$ ratio to give a total flow rate of 10 mL $min^{-1}$ (3 mL $min^{-1}$ $C_3H_8$, 7 mL $min^{-1}$ 20 % $O_2$/80 % He by volume), and spectra were continuously recorded. Representative normalized spectra at 80, 240, and 440 minutes on stream, and after reaction are shown in Figure 1c. After 120 minutes on stream, the total flow rate was decreased to 7 mL $min^{-1}$ (2 mL $min^{-1}$ $C_3H_8$, 5 mL $min^{-1}$ air) to increase the contact time. The reaction proceeded until a steady amount of oxidized boron had formed (8 h total reaction time). The sample was then cooled to room temperature in air, heated back up to 500 °C, and re-exposed to reaction conditions for an additional 105 min before being cooled to end the experiment. When propane was added to the hot catalyst, the MS signal for the ODH reaction product $H_2O$ (m/z = 18) appeared with a slight delay relative to the signals for propane (m/z = 28 and 44), indicating that ODHP was occurring (Figure S3). The MS signals for propylene overlap

with those for propane and are thus not a clear indicator of the reaction proceeding.

Two features at 192 eV and 194 eV are observed in the postreaction spectrum (green trace in Figure 1c). As seen in Figure 1b, the peak at 192 eV corresponds to [$BN_3$] species and the peak at 194 eV corresponds to [$BO_3$]-type species. The intensity of the [$BO_3$] feature increases over the course of the reaction. The area under the 192 eV and 194 eV signals was integrated, and the resulting percentage areas over the course of the experiment are plotted in Figure 1d (plot of integrated area over time is shown in Figure S4). With a total flow rate of 10 mL $min^{-1}$, there is a slow increase in the amount of oxidized boron. When the flow rate is decreased to 7 mL $min^{-1}$, increasing the contact time, the amount of oxide initially decreases then quickly increases, eventually reaching a maximum of *ca.* 25% of the total integrated area. This value is in line with previous quantification by solid state NMR (SSNMR), which shows that hBN after reaction contains 30% [$BO_3$]-type species.[8] There is little change in surface composition upon re-exposure to reaction conditions, indicating the surface has reached a steady state composition.

Linear combination fitting (LCF) analysis was applied to quantify the relative amount of the two species present using the spectra of hBNNS and $B_2O_3$ acquired at room temperature as standards. The LCF results (Figure S5) show the same trend as the percentage areas in Figure 1. Fitting the [$BO_3$] peak at 194 eV with the $B_2O_3$ standard consistently shows a residual at the lower energy side of the experimental peak (Figure S6). This residual is present both at room and reaction temperatures, although the intensity of the residual peak is larger at elevated temperatures (Figure S6a). The residual in the oxide feature suggests the presence of boron oxyhydroxide species with geometry and coordination distinct from the boron species in $B_2O_3$. The presence of distinct boron oxyhydroxide species is in line with proposed structures from SSNMR as well as with theory-predicted metastable $BO_x$ species. The [$BN_3$] peak at 192 eV also exhibits residuals, but only at elevated temperatures (Figure S6b). These residuals are associated with distortions in the hBN layer due to oxidation of facial sites (as opposed to edge sites) (Figure S7), especially the highly restructured facial species whose populations only become significant at reaction temperatures. Proposed structures from theory which may account for the subtle spectral changes observed under reaction conditions are discussed in detail below.

Interestingly, when the flow rate is decreased, the oxide temporarily disappears (at 160 min.), reappearing in the next averaged spectral time (*i.e.,* the oxide was not present for *ca.* 40 min.). Decreasing the gas flow rate increases the contact time and therefore the conversion, leading to an increased local concentration of water. As water has been shown to hydrolyze boron oxide, an explanation for the temporary loss of the [$BO_3$] signal is that the species were hydrolyzed, and the re-oxidation of hBN is slow at this stage of the reaction.

We confirmed our observations in a second repeat experiment (Figure S8). Our results show that once the oxidized boron layer is formed, the surface structure, though dynamic on the short time scale,[11] is stable on the time scale of XRS. The success of XRS in tracking oxyfunctionalization allowed us to design experiments that could reveal more about the behavior of the active phase, such as the effect of a water cofeed on the surface. Therefore, to better understand the active oxide phase, we perturbed the system by modulating water addition into the reaction mixture.

**Probing the Effect of Water Vapor on the Catalyst Surface.** As mentioned above, the addition of water vapor to the ODH feed has previously been shown to enhance the rate of propane conversion.[25] The enhancement effect is reversible, and it was hypothesized that the main roles of water are to: (i) increase the radical pool concentration, and (ii) assist in the rate determining step of active site regeneration. Here, we probe the effect of water vapor on the hBN catalyst while simultaneously monitoring the reaction products by gas chromatography (GC).

hBNNS (powdered and undiluted, from the same batch used in Figure 1) was packed into a 1mm o.d. capillary tube to give a 10 mm catalyst bed length and mounted at BL 15-2 at SSRL. The sample was heated in synthetic air (at 10 °C/min) to 550 °C before switching to a dry reaction gas mix (*i.e.,* without any added water) until a stable amount of [$BO_3$] (194 eV feature) formed. Following the induction period, the gas was routed through the room temperature water saturator to start the first wet cycle. After about 80 minutes, the gas feed was switched back to the dry feed. The wet and dry cycles were performed twice.

Normalized B K-edge X-ray Raman spectra collected throughout the cofeeding experiment are shown in Figure S9. The area under the peaks at 192 eV and 194 eV of the individual normalized B K-edge XRS scans were integrated, and the resulting percentage areas are plotted over time in Figure 2a (integrated areas shown in Figure S10). Figure 2b shows the propylene production rate over the course of the reaction. Representative GC traces are shown in Figure S11. In each of the plots in Figure 2, the blue shading indicates a wet cycle, and the beige shading indicates a dry cycle. LCF analysis was also performed on these spectra (Figure S12). As in the previous experiment, there is a residual present at the lower energy side of the 194 eV peak that corresponds to [$BO_3$]-type species (Figure S13).

As was shown in Figure 1 for the dry feed, there is again a gradual increase in the 194 eV feature ([$BO_3$]-type species) during the induction period until a stable surface composition is formed (first beige segment in Figure 2a). When water is added to the feed (first blue segment in Figure 2), the oxide feature at 194 eV quickly disappears. Upon the removal of water from the gas feed, the 194 eV signal gradually returns, showing that the removal of boron oxyhydroxide can be cycled. Oxide removal occurs faster than oxide growth, with removal occurring within the first 10 minutes of a wet cycle and growth occurring after at least 15 minutes of a dry cycle (Figure 2a). The propylene production rate (Figure 2b) is lower in the wet cycles than in the dry cycles, a trend opposite to that observed by Venegas, *et al.*[25]

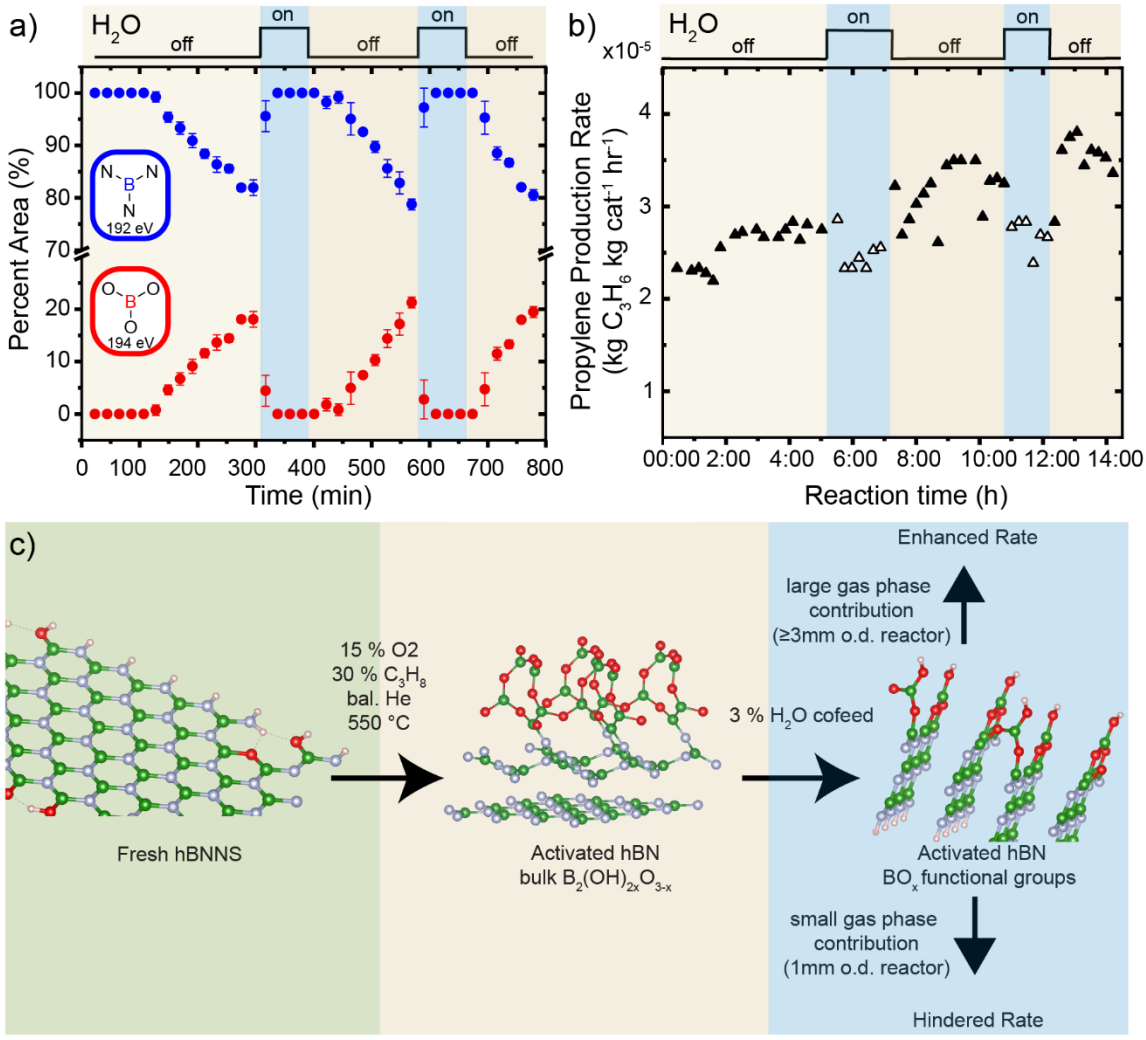


**Figure 2.** (a) integrated areas of the $BN_3$ (blue circles) and $BO_3$ (red circles) features over the time of the experiment; and (b) propylene production rate over time. Reaction conditions: T = 550 °C, 10 mL $min^{-1}$ total flow rate (1.4 mL $min^{-1}$ $C_3H_8$, 3.5 mL $min^{-1}$ 20% $O_2$/He, 5.1 mL $min^{-1}$ He). The beige shaded regions indicate a dry cycle (no added water), and the blue shaded regions indicate a wet cycle (with 3% cofed water). (c) Scheme summarizing the surface response to the conditions probed in the water cofeed experiments. The error bars in (a) are the standard deviation determined from averaging 3 to 5 individual scans.

The removal of boron oxyhydroxide by water is consistent with a previous study where the active boron oxyhydroxide layer is hydrolyzed from silica-supported catalysts in a post-reaction washing step.[13] However, the catalytic response to the addition of water was initially surprising, aslab-based results show an increase in propylene production as a result of the water cofeed. Based on the inverse relationship to water addition seen in our reactivity results measured at BL 15-2 and the hypothesis that a role of water is to increase the radical pool concentration, we hypothesize that the differing response is an effect of minimal gas phase contribution in the 1mm reactor configuration used for the XRS study. Work from Venegas, *et al.*, demonstrated the importance of reactor parameters on the reaction rate for ODHP over hBN.[24] They observed a drastic decrease in ODHP activity for hBN in a 4mm inner diameter (i.d.) reactor compared to an 8 mm i.d. reactor tube at similar contact times and showed that propane conversion scales linearly with the void volume of the catalyst bed.

In our cofeed experiment at BL 15-2, the catalyst was packed into a 1mm outer diameter (o.d.) capillary to give a 10 mm length bed (bed volume: ≈8 $mm^3$), a volume that is two orders of magnitude smaller than that in typical laboratory-based reactors (bed volume for 6mm i.d. reactor used in Venegas, *et al.*: 570 $mm^3$).[25] To test our hypothesis, we performed water cofeeding experiments using a 3 mm o.d. capillary tube (10 mm length bed, bed volume: ≈71 $mm^3$). Similar to our beamline experiments, the hBN catalyst was treated at 550 °C under a dry reaction mix for 8 hours to form the stable oxide phase. When water was cofed into the reactor, we observed the expected enhancement to the reaction rate (Figure S14). Notably, there was visible white deposit at the outlet of the 3mm capillary reactor at the end of the water cofeed experiments, indicating that boron was

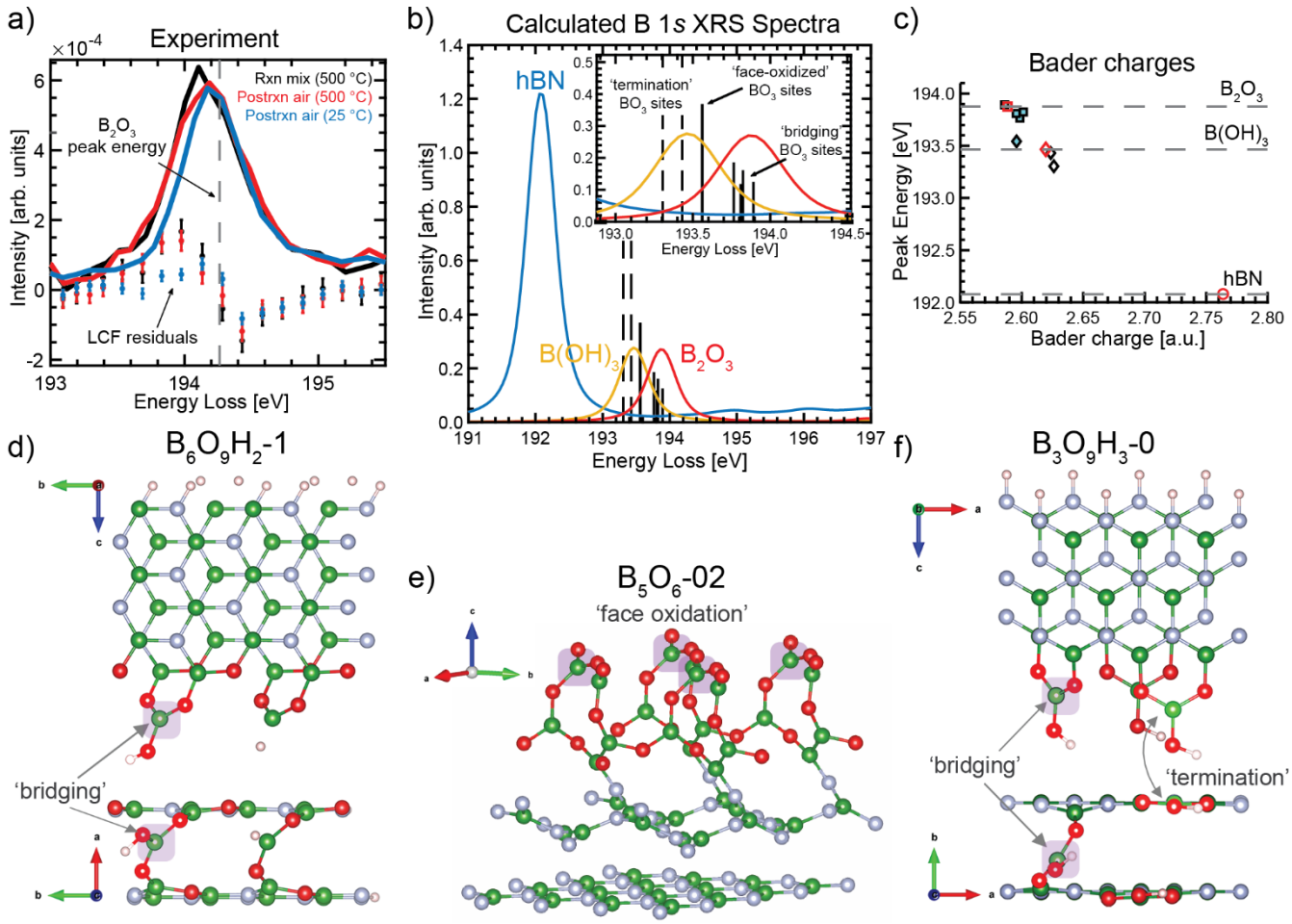


**Figure 3.** a) Experimental B 1*s* XRS spectra zoomed in on the 194 eV feature ($BO_3$-type species) of hBNNS under the reaction gas mix (30% $C_3H_8$, 15% $O_2$, bal. He) at 500 °C (black line), under air at 500 °C (red line), and under air at 25 °C (blue line); markers with error bars are the corresponding LCF residuals. The black dashed line indicates the reference $B_2O_3$ peak energy from experiment. b) Calculated B 1s XRS spectra of hBN, $B(OH)_3$, and $B_2O_3$ along with peak energies of $BO_3$-type sites within relevant structures under ODH of propane. c) Bader charges and Peak energies of candidate boron structures and references. References – red markers: hBN (open red circle), $B(OH)_3$ (open red diamond) and $B_2O_3$ (open red square). Candidate structures $BO_3$-sites: 'termination' (open black diamond), 'face-oxidized' (filled cyan diamond), 'bridging' (filled cyan squares). d-f) Representative candidate structures.

hydrolyzed from the surface as in the 1mm capillary reactor (Figure S15). The observed enhancement by water along with boron oxide hydrolysis in the larger volume catalyst bed supports our hypothesis of minimal gas phase contribution in the 1mm capillary reactor. We can therefore ascribe the reactivity we observe in the1mm reactor to the surface alone. Thus, when the reactor volume in sufficiently large and gas phase chemistry is present, water enhances the reaction rate; when reactor volume is small and gas phase chemistry is not present, the surface reactivity dominates, and water hinders the reaction rate. In both cases, water removes oxidized boron from the catalyst.

Propylene production does not completely stop with the loss of the [$BO_3$] XRS signal, indicating that there are residual [$BO_3$] functional groups able to perform the reaction. However, the loss in propylene production rate is not proportional to the loss of oxide content, which is likely an effect of the ability of water to assist in the rate determining step of active site regeneration. So, although water has removed the bulk boron oxyhydroxide, leading to decreased propylene production, functional groups which can perform the reaction remain and their regeneration is aided by the presence of water. To confirm the presence of residual boron oxyhydroxide, $^{11}B$ SSNMR of activated hBN treated with a water cofeed (in a 7mm i.d. reactor) shows the presence of *ca.* 10% [$BO_3$]-type species (Figure S16), a relative oxide contribution much lower than the 30% [$BO_3$]-type species previously reported for activated hBN without a water cofeed.[8] Additionally, the volume-dependent response to water indicates that under typical laboratory reactor conditions, the gas phase chemistry is more kinetically relevant than the surface chemistry.

**Structural Insights from Theory.** As mentioned above, LCF analysis using hBN and $B_2O_3$ standards results in residuals around both the [$BN_3$] peak at 192 eV and the [$BO_3$] feature at 194 eV. For the [$BN_3$] peak, residuals are observed only at high temperatures, whereas for the [$BO_3$] feature, a small residual is present at room which becomes more prominent at elevated temperatures (Figure 3a). To understand this behavior, we investigated

the surface reconstruction of h-BN edges and faces under ODHP conditions by performing systematic simulations of X-Ray Raman spectra for several candidate structures and references (Figure 3b, see SI for calculation details). The peak energy as a function of Bader charge is shown in Figure 3c. The candidate structures (Figure 3d-f) are partially oxidized/hydroxylated and restructured h-BN terminations (armchair edge, zigzag edge, and face) from grand canonical global optimization sampling, with varying surface stoichiometry of $B_xO_yH_z$. Notably, this method captures not only the structures of the most stable surface phase (global minimum), but also the metastable structures (local minima) which are only accessible in the catalytic conditions, such as the bridged O-B-O over the h-BN edges and the unsaturated B-B motifs on restructured h-BN faces.

The obtained ensemble of reconstructed face-oxidized structures predicts the formation of different boron species on top of the hBN layer, introducing structural changes and distortions in the upper hBN lattice (Figure 3e). Therefore, the overall distance between the undistorted and top (oxidized) layer becomes smaller as compared to edge-oxidation or pristine hBN (Figure S7b and c). Particularly, the distance between nearest boron atoms at adjacent layers for hBN and edge-oxidation structures is approximately ≈3.62 Å and ≈3.65 Å, respectively, whereas for face-oxidated structures this distance can get as small as ≈2.78 Å. Such reduction in the interlayer distance yields additional spectral features on the low- and high-energy sides of the [$BN_3$] peak, distorting the characteristic single peak observed in hBN and edge-oxidation candidates (Figure S7b-d). In edge-oxidation structure candidates, we found that the only species giving additional features in the near vicinity of the [$BN_3$] energy peak are [$BO_2H$] and [$BN_2O$] sites for the edge-armchair and edge-zigzag structures, respectively. From the above results, we found that the reduction in the interlayer distance due to face-oxidation and the presence of [$BO_2H$] and [$BN_2O$] species in edge-oxidation candidates, both occurring at reaction conditions and/or high temperatures, are the most probable cause accounting for the experimental changes observed at the [$BN_3$] feature at high-temperatures.

Several boron species are formed at the reconstructed hBN termination edges. Energy positions of the first resonance (peak energies) *vs* Bader charges of these boron sites along with reference structures are shown in Figure S17. An almost linear relation is observed between the peak energies and Bader charges of the different boron sites, particularly for the armchair-edge candidates and a relatively larger dispersion on the results for the zigzag-edge structures (Figure S17 (b)). Overall, the calculations exhibit a remarkable consistency across all considered structures, showing the reliability of the DFT-BSE approach implemented in OCEAN[43] for predicting relative energy positions of spectral features between different systems. From all oxidized boron species present within these structures, only [$BO_3$] sites have peak energies with values ranging from the vicinity of $B(OH)_3$ up to $B_2O_3$ reference systems. The more symmetric and strained ones – those [$BO_3$] sites where two oxygens are bonded to boron atoms of the same hBN layer, labeled as 'termination' sites (Figure 3f) – have peak energies below the $B(OH)_3$ peak. More interestingly, only those [$BO_3$] sites 'bridging' between two adjacent layers (Figure 3d and f), where two of the oxygens are bonded to boron atoms in different hBN layers, have peak energies above $B(OH)_3$ and close to $B_2O_3$. It is precisely in this energy range where the experiment shows the largest residuals of the LCF fitting around the oxide peak at reaction conditions (Figure 3a).

The difference between the 'bridging' species in the edge-zigzag and edge-armchair candidate structures, is in the chemical environment of the termination layer boron site where the bridge is connected. For edge-armchair and edge-zigzag the termination boron atoms linking the bridging species are [$BO_2N$] and [$BN_2O$] sites, respectively. This difference becomes very relevant when considering that, according to our calculations, [$BO_2N$] sites would yield spectral features at ≈1 eV above the [$BN_3$] peak (Figure S17 (b)). However, in the experiment there is no evidence of such features at any measured condition. Hence, these observations allow us to rationalize that, during *operando* conditions, only [$BO_3$] 'bridging' sites between zigzag-edge terminations are fully compatible with the evolution of the observed experimental features at both [$BN_3$] and [$BO_3$] peaks and accounts for spectral the changes during reaction. Another structure yielding boron oxides with peak energies in this energy region, though slightly below [$BO_3$] 'bridging' species, are those [$BO_3$] sites formed in the upper layer during 'face-oxidation' (Figure 3e). These results are summarized in Figure 3.

## CONCLUSIONS

We performed an *operando* X-Ray Raman spectroscopy study to observe the oxyfunctionalization of hBN during the catalyst start-up in the ODH of propane. We then used *operando* XRS to clarify the role of cofed water in hBN-catalyzed ODHP. When water is added into the reaction gas feed, the peak for [$BO_3$] disappears and the rate of propylene formation decreases. The reactivity response is the opposite of the rate enhancement effect by water addition previously reported in the literature. We show that the different response in activity is an effect of the smaller reactor volume which minimizes the gas phase contribution. Therefore, the reactivity observed during the *operando* XRS study is dominated by the surface with minimal contributions from the gas phase. When gas phase chemistry participates, water enhances the rate of reaction; when the gas phase chemistry does not participate, water hinders the reaction rate. In both cases, water removes oxidized boron from the surface. Under typical laboratory reactor conditions, the effect of water on the gas phase is greater than its effect on the surface, and the gas phase chemistry is responsible for the majority of the observed conversion. These novel results showcase the unique ability of XRS for the *operando* characterization of boron-based (or other low-Z) catalysts under relevant reaction environments. Importantly, the demonstrated high accuracy of the simulated XRS spectra highlights the unprecedented value of state-of-the-art theoretical approaches. Altogether, such experimental-theoretical tools are now setting a new era for *operando* catalysis research as they can rationalize with high fidelity spectral fingerprint originating from transient complex structures

that cannot be obtained experimentally from standard materials or *ex-situ* studies.

## ASSOCIATED CONTENT

**Supporting Information**. Experimental methods, computational details, and additional characterization and results. This material is available free of charge via the Internet at http://pubs.acs.org.

## AUTHOR INFORMATION

### Corresponding Author

*Ive Hermans Department of Chemistry, University of Wisconsin – Madison, Madison, Wisconsin 53706, United States; Department of Chemical and Biological Engineering, University of Wisconsin – Madison, Madison, Wisconsin 53706, United States ; Wisconsin Energy Institute, University of Wisconsin – Madison, Madison, Wisconsin, 53706, United States;
email: hermans@chem.wisc.edu
*Simon R. Bare Stanford Synchrotron Radiation Lightsource, SLAC National Accelerator Laboratory, Menlo Park, California 94025, United States
Email: srbare@slac.stanford.edu
*Dimosthenis Sokaras *Stanford Synchrotron Radiation Lightsource, SLAC National Accelerator Laboratory, Menlo Park, California 94025, United States*
email: dsokaras@slac.stanford.edu

### Present Addresses

†M.C.C. present address: Stanford Synchrotron Radiation Lightsource, SLAC National Accelerator Laboratory, Menlo Park, California 94025, United States

### Author Contributions

‡These authors contributed equally.
All authors have given approval to the final version of the manuscript.

### Notes

The authors declare no competing financial interests.

## ACKNOWLEDGMENT

M.C.C. was supported by the DOE BES, Office of Workforce Development for Teachers and Scientists, Office of Science Graduate Student Research (SCGSR) program, which is administered by the Oak Ridge Institute for Science and Education for the DOE under contract number DE-SC0014664. This research used resources of the Stanford Synchrotron Radiation Lightsource. Use of the Stanford Synchrotron Radiation Lightsource, SLAC National Accelerator Laboratory, is supported by the U.S. Department of Energy, Office of Science, Office of Basic Energy Sciences under Contract No. DE-AC02-76SF00515. Co-ACCESS is supported by the U.S. Department of Energy, Office of Basic Energy Sciences, Chemical Sciences, Geosciences and Biosciences Division. Catalytic and mechanistic investigations of boron-based ODH catalysts was supported by DOE BES under award DE-SC0017918. The Bruker AVANCE III 500 NMR spectrometer was supported by the Bender Fund and UW2020. Z.Z. and A.N.A. acknowledge U.S. DOE, Office of Science, Basic Energy Science Program for financial support under the grant number DE-SC0019152. The computations in this work were performed on Hoffman2 the UCLA-shared cluster; Cori and Perlmutter of the National Energy Research Scientific Computing Center (NERSC), a U.S. Department of Energy Office of Science User Facility operated under Contract DE-AC02-05CH11231; Theta of the Innovative and Novel Computational Impact on Theory and Experiment (INCITE) program at the Argonne Leadership Computing Facility, a U.S. Department of Energy Office of Science User Facility operated under Contract DE-AC02-06CH11357.

## REFERENCES

(1) Grant, J. T.; Carrero, C. A.; Goeltl, F.; Venegas, J.; Mueller, P.; Burt, S. P.; Specht, S. E.; McDermott, W. P.; Chieregato, A.; Hermans, I. Selective Oxidative Dehydrogenation of Propane to Propene Using Boron Nitride Catalysts. *Science* **2016**, *354* (6319), 1570–1573. https://doi.org/10.1126/science.aaf7885.

(2) Grant, J. T.; McDermott, W. P.; Venegas, J. M.; Burt, S. P.; Micka, J.; Phivilay, S. P.; Carrero, C. A.; Hermans, I. Boron and Boron-Containing Catalysts for the Oxidative Dehydrogenation of Propane. *ChemCatChem* **2017**, *9* (19), 3623–3626. https://doi.org/10.1002/cctc.201701140.

(3) Huang, R.; Zhang, B.; Wang, J.; Wu, K.-H.; Shi, W.; Zhang, Y.; Liu, Y.; Zheng, A.; Schlögl, R.; Su, D. S. Direct Insight into Ethane Oxidative Dehydrogenation over Boron Nitrides. *ChemCatChem* **2017**, *9* (17), 3293–3297. https://doi.org/10.1002/cctc.201700725.

(4) Shi, L.; Wang, D.; Song, W.; Shao, D.; Zhang, W.-P.; Lu, A.-H. Edge-Hydroxylated Boron Nitride for Oxidative Dehydrogenation of Propane to Propylene. *ChemCatChem* **2017**, *9* (10), 1788–1793. https://doi.org/10.1002/cctc.201700004.

(5) Rightor, E. G.; Tway, C. L. Global Energy & Emissions Reduction Potential of Chemical Process Improvements. *Catal. Today* **2015**, *258*, 226–229. https://doi.org/10.1016/j.cattod.2015.02.023.

(6) Cavani, F.; Ballarini, N.; Cericola, A. Oxidative Dehydrogenation of Ethane and Propane: How Far from Commercial Implementation? *Catal. Today* **2007**, *127* (1–4), 113–131. https://doi.org/10.1016/j.cattod.2007.05.009.

(7) Love, A. M.; Cendejas, M. C.; Thomas, B.; McDermott, W. P.; Uchupalanun, P.; Kruszynski, C.; Burt, S. P.; Agbi, T.; Rossini, A. J.; Hermans, I. Synthesis and Characterization of Silica-Supported Boron Oxide Catalysts for the Oxidative Dehydrogenation of Propane. *J. Phys. Chem. C* **2019**, *123* (44), 27000–27011. https://doi.org/10.1021/acs.jpcc.9b07429.

(8) Love, A. M.; Thomas, B.; Specht, S. E.; Hanrahan, M. P.; Venegas, J. M.; Burt, S. P.; Grant, J. T.; Cendejas, M. C.; McDermott, W. P.; Rossini, A. J.; Hermans, I. Probing the Transformation of Boron Nitride Catalysts under Oxidative Dehydrogenation Conditions. *J. Am. Chem. Soc.* **2019**, *141* (1), 182–190. https://doi.org/10.1021/jacs.8b08165.

(9) Dorn, R. W.; Cendejas, M. C.; Chen, K.; Hung, I.; Altvater, N. R.; McDermott, W. P.; Gan, Z.; Hermans, I.; Rossini, A. J. Structure Determination of Boron-Based Oxidative Dehydrogenation Heterogeneous Catalysts With Ultrahigh Field 35.2 T $^{11}$B Solid-State NMR Spectroscopy. *ACS Catal.* **2020**, *10* (23), 13852–13866. https://doi.org/10.1021/acscatal.0c03762.

(10) Schmatz-Engert, P.; Herold, F.; Heinschke, S.; Totzauer, L.; Hofmann, K.; Drochner, A.; Weidenkaff, A.; Schneider, J. J.; Albert, B.; Qi, W.; Etzold, B. J. M. Oxygen-Functionalized

Boron Nitride for the Oxidative Dehydrogenation of Propane – The Case for Supported Liquid Phase Catalysis. *ChemCatChem* **2022**, *14* (8). https://doi.org/10.1002/cctc.202200068.

(11) Zhang, Z.; Jimenez-Izal, E.; Hermans, I.; Alexandrova, A. N. Dynamic Phase Diagram of Catalytic Surface of Hexagonal Boron Nitride under Conditions of Oxidative Dehydrogenation of Propane. *J. Phys. Chem. Lett.* **2019**, *10* (1), 20–25. https://doi.org/10.1021/acs.jpclett.8b03373.

(12) Zhang, Z.; Hermans, I.; Alexandrova, A. N. Off-Stoichiometric Restructuring and Sliding Dynamics of Hexagonal Boron Nitride Edges in Conditions of Oxidative Dehydrogenation of Propane. *J. Am. Chem. Soc.* **2023**, jacs.3c04613. https://doi.org/10.1021/jacs.3c04613.

(13) Lu, W.-D.; Wang, D.; Zhao, Z.; Song, W.; Li, W.-C.; Lu, A.-H. Supported Boron Oxide Catalysts for Selective and Low-Temperature Oxidative Dehydrogenation of Propane. *ACS Catal.* **2019**, *9* (9), 8263–8270. https://doi.org/10.1021/acscatal.9b02284.

(14) Altvater, N. R.; Dorn, R. W.; Cendejas, M. C.; McDermott, W. P.; Thomas, B.; Rossini, A. J.; Hermans, I. B-MWW Zeolite: The Case Against Single-Site Catalysis. *Angew. Chem. Int. Ed.* **2020**, *59* (16), 6546–6550. https://doi.org/10.1002/anie.201914696.

(15) Belgamwar, R.; Rankin, A. G. M.; Maity, A.; Mishra, A. K.; Gómez, J. S.; Trébosc, J.; Vinod, C. P.; Lafon, O.; Polshettiwar, V. Boron Nitride and Oxide Supported on Dendritic Fibrous Nanosilica for Catalytic Oxidative Dehydrogenation of Propane. *ACS Sustain. Chem. Eng.* **2020**, *8* (43), 16124–16135. https://doi.org/10.1021/acssuschemeng.0c04148.

(16) Qiu, B.; Jiang, F.; Lu, W.-D.; Yan, B.; Li, W.-C.; Zhao, Z.-C.; Lu, A.-H. Oxidative Dehydrogenation of Propane Using Layered Borosilicate Zeolite as the Active and Selective Catalyst. *J. Catal.* **2020**, *385*, 176–182. https://doi.org/10.1016/j.jcat.2020.03.021.

(17) Si, C.; Lian, Z.; Olanrele, S. O.; Sun, X.; Li, B. Revealing the Origin of the Reactivity of Metal-Free Boron Nitride Catalysts in Oxidative Dehydrogenation of Propane. *Appl. Surf. Sci.* **2020**, *519*, 146241. https://doi.org/10.1016/j.apsusc.2020.146241.

(18) Cendejas, M. C.; Dorn, R. W.; McDermott, W. P.; Lebrón-Rodríguez, E. A.; Mark, L. O.; Rossini, A. J.; Hermans, I. Controlled Grafting Synthesis of Silica-Supported Boron for Oxidative Dehydrogenation Catalysis. *J. Phys. Chem. C* **2021**, *125* (23), 12636–12649. https://doi.org/10.1021/acs.jpcc.1c01899.

(19) Liu, Z.; Yan, B.; Meng, S.; Liu, R.; Lu, W.; Sheng, J.; Yi, Y.; Lu, A. Plasma Tuning Local Environment of Hexagonal Boron Nitride for Oxidative Dehydrogenation of Propane. *Angew. Chem. Int. Ed.* **2021**, *60* (36), 19691–19695. https://doi.org/10.1002/anie.202106713.

(20) Mark, L. O.; Dorn, R. W.; McDermott, W. P.; Agbi, T. O.; Altvater, N. R.; Jansen, J.; Lebrón-Rodríguez, E. A.; Cendejas, M. C.; Rossini, A. J.; Hermans, I. Highly Selective Carbon-Supported Boron for Oxidative Dehydrogenation of Propane. *ChemCatChem* **2021**, *13* (16), 3611–3618. https://doi.org/10.1002/cctc.202100759.

(21) Yan, H.; Alayoglu, S.; Wu, W.; Zhang, Y.; Weitz, E.; Stair, P. C.; Notestein, J. M. Identifying Boron Active Sites for the Oxidative Dehydrogenation of Propane. *ACS Catal.* **2021**, *11* (15), 9370–9376. https://doi.org/10.1021/acscatal.1c02168.

(22) Zhou, H.; Yi, X.; Hui, Y.; Wang, L.; Chen, W.; Qin, Y.; Wang, M.; Ma, J.; Chu, X.; Wang, Y.; Hong, X.; Chen, Z.; Meng, X.; Wang, H.; Zhu, Q.; Song, L.; Zheng, A.; Xiao, F.-S. Isolated Boron in Zeolite for Oxidative Dehydrogenation of Propane. *Science* **2021**, *372* (6537), 76–80. https://doi.org/10.1126/science.abe7935.

(23) Venegas, J. M.; Grant, J. T.; McDermott, W. P.; Burt, S. P.; Micka, J.; Carrero, C. A.; Hermans, I. Selective Oxidation of *n* -Butane and Isobutane Catalyzed by Boron Nitride. *ChemCatChem* **2017**, *9* (12), 2118–2127. https://doi.org/10.1002/cctc.201601686.

(24) Venegas, J. M.; Hermans, I. The Influence of Reactor Parameters on the Boron Nitride-Catalyzed Oxidative Dehydrogenation of Propane. *Org. Process Res. Dev.* **2018**, *22* (12), 1644–1652. https://doi.org/10.1021/acs.oprd.8b00301.

(25) Venegas, J. M.; Zhang, Z.; Agbi, T. O.; McDermott, W. P.; Alexandrova, A.; Hermans, I. Why Boron Nitride Is Such a Selective Catalyst for the Oxidative Dehydrogenation of Propane. *Angew. Chem. Int. Ed.* **2020**, *59* (38), 16527–16535. https://doi.org/10.1002/anie.202003695.

(26) Kraus, P.; Lindstedt, R. P. It's a Gas: Oxidative Dehydrogenation of Propane over Boron Nitride Catalysts. *J. Phys. Chem. C* **2021**, *125* (10), 5623–5634. https://doi.org/10.1021/acs.jpcc.1c00165.

(27) McDermott, W. P.; Venegas, J.; Hermans, I. Selective Oxidative Cracking of *N*- Butane to Light Olefins over Hexagonal Boron Nitride with Limited Formation of $CO_x$. *ChemSusChem* **2020**, *13* (1), 152–158. https://doi.org/10.1002/cssc.201901663.

(28) Zhang, X.; You, R.; Wei, Z.; Jiang, X.; Yang, J.; Pan, Y.; Wu, P.; Jia, Q.; Bao, Z.; Bai, L.; Jin, M.; Sumpter, B.; Fung, V.; Huang, W.; Wu, Z. Radical Chemistry and Reaction Mechanisms of Propane Oxidative Dehydrogenation over Hexagonal Boron Nitride Catalysts. *Angew. Chem. Int. Ed.* **2020**, *59* (21), 8042–8046. https://doi.org/10.1002/anie.202002440.

(29) Zhang, Z.; Tian, J.; Wu, X.; Surin, I.; Pérez-Ramírez, J.; Hemberger, P.; Bodi, A. Unraveling Radical and Oxygenate Routes in the Oxidative Dehydrogenation of Propane over Boron Nitride. *J. Am. Chem. Soc.* **2023**, *145* (14), 7910–7917. https://doi.org/10.1021/jacs.2c12970.

(30) Bergmann, U.; Glatzel, P.; Cramer, S. P. Bulk-Sensitive XAS Characterization of Light Elements: From X-Ray Raman Scattering to X-Ray Raman Spectroscopy. *Microchem. J.* **2002**, *71* (2–3), 221–230. https://doi.org/10.1016/S0026-265X(02)00014-0.

(31) Sokaras, D.; Nordlund, D.; Weng, T.-C.; Mori, R. A.; Velikov, P.; Wenger, D.; Garachtchenko, A.; George, M.; Borzenets, V.; Johnson, B.; Qian, Q.; Rabedeau, T.; Bergmann, U. A High Resolution and Large Solid Angle X-Ray Raman Spectroscopy End-Station at the Stanford Synchrotron Radiation Lightsource. *Rev. Sci. Instrum.* **2012**, *83* (4), 043112. https://doi.org/10.1063/1.4704458.

(32) Tohji, K.; Udagawa, Y. X-Ray Raman Scattering as a Substitute for Soft-x-Ray Extended x-Ray-Absorption Fine Structure. *Phys. Rev. B* **1989**, *39* (11), 7590–7594. https://doi.org/10.1103/PhysRevB.39.7590.

(33) Schülke, W. *Electron Dynamics by Inelastic X-Ray Scattering*; Oxford series on synchrotron radiation; Oxford University Press: Oxford ; New York, 2007.

(34) Miedema, P. S.; Ngene, P.; van der Eerden, A. M. J.; Weng, T.-C.; Nordlund, D.; Sokaras, D.; Alonso-Mori, R.; Juhin, A.; de Jongh, P. E.; de Groot, F. M. F. In Situ X-Ray Raman Spectroscopy of LiBH4. *Phys. Chem. Chem. Phys.* **2012**, *14* (16), 5581. https://doi.org/10.1039/c2cp24025d.

(35) Miedema, P. S.; Ngene, P.; van der Eerden, A. M. J.; Sokaras, D.; Weng, T.-C.; Nordlund, D.; Au, Y. S.; de Groot, F. M. F. In Situ X-Ray Raman Spectroscopy Study of the Hydrogen Sorption Properties of Lithium Borohydride Nanocomposites. *Phys Chem Chem Phys* **2014**, *16* (41), 22651–22658. https://doi.org/10.1039/C4CP02918F.

(36) Braun, A.; Nordlund, D.; Song, S.-W.; Huang, T.-W.; Sokaras, D.; Liu, X.; Yang, W.; Weng, T.-C.; Liu, Z. Hard X-Rays in–Soft X-Rays out: An Operando Piggyback View Deep into a Charging Lithium Ion Battery with X-Ray Raman Spectroscopy. *J. Electron Spectrosc. Relat. Phenom.* **2015**, *200*, 257–263. https://doi.org/10.1016/j.elspec.2015.03.005.

(37) Ketenoglu, D.; Spiekermann, G.; Harder, M.; Oz, E.; Koz, C.; Yagci, M. C.; Yilmaz, E.; Yin, Z.; Sahle, C. J.; Detlefs, B.; Yavaş, H. X-Ray Raman Spectroscopy of Lithium-Ion Battery Electrolyte Solutions in a Flow Cell. *J. Synchrotron Radiat.* **2018**, *25* (2), 537–542. https://doi.org/10.1107/S1600577518001662.

(38) Boesenberg, U.; Sokaras, D.; Nordlund, D.; Weng, T.-C.; Gorelov, E.; Richardson, T. J.; Kostecki, R.; Cabana, J. Electronic Structure Changes upon Lithium Intercalation into Graphite – Insights from Ex Situ and Operando x-Ray Raman Spectroscopy. *Carbon* **2019**, *143*, 371–377. https://doi.org/10.1016/j.carbon.2018.11.031.

(39) Moya-Cancino, J. G.; Honkanen, A.-P.; van der Eerden, A. M. J.; Oord, R.; Monai, M.; ten Have, I.; Sahle, C. J.; Meirer, F.; Weckhuysen, B. M.; de Groot, F. M. F.; Huotari, S. *In Situ* X-Ray Raman Scattering Spectroscopy of the Formation of Cobalt Carbides in a Co/$TiO_2$ Fischer–Tropsch Synthesis Catalyst. *ACS Catal.* **2021**, *11* (2), 809–819. https://doi.org/10.1021/acscatal.0c04509.

(40) Hoffman, A. S.; Singh, J. A.; Bent, S. F.; Bare, S. R. *In Situ* Observation of Phase Changes of a Silica-Supported Cobalt Catalyst for the Fischer–Tropsch Process by the Development of a Synchrotron-Compatible *in Situ/Operando* Powder X-Ray Diffraction Cell. *J. Synchrotron Radiat.* **2018**, *25* (6), 1673–1682. https://doi.org/10.1107/S1600577518013942.

(41) Watanabe, N.; Hayashi, H.; Udagawa, Y.; Takeshita, K.; Kawata, H. Anisotropy of Hexagonal Boron Nitride Core Absorption Spectra by X-ray Raman Spectroscopy. *Appl. Phys. Lett.* **1996**, *69* (10), 1370–1372. https://doi.org/10.1063/1.117439.

(42) Feng, Y.; Soininen, J. A.; Ankudinov, A. L.; Cross, J. O.; Seidler, G. T.; Macrander, A. T.; Rehr, J. J.; Shirley, E. L. Exciton Spectroscopy of Hexagonal Boron Nitride Using Nonresonant X-Ray Raman Scattering. *Phys. Rev. B* **2008**, *77* (16), 165202. https://doi.org/10.1103/PhysRevB.77.165202.

(43) Vinson, J. Advances in the OCEAN -3 Spectroscopy Package. *Phys. Chem. Chem. Phys.* **2022**, *24* (21), 12787–12803. https://doi.org/10.1039/D2CP01030E.

Table of Contents (TOC)